Bulk coupling of polarization and magnetism in the hexagonal ferrites

Hena Das, Aleksander L. Wysocki and Craig J. Fennie
School of Applied and Engineering Physics, Cornell University, Ithaca, NY, USA

(Dated: February 6, 2013)

The interplay of improper structural ferroelectricity (trimerization) and geometrically frustrated spins in the hexagonal $RMnO_3$ rare-earth manganites lead to a network of topologically protected defects that create strongly coupled structural and magnetic vortices. This unusual vortex structure is responsible for a significant domain wall magnetoelectric effect and magnetization, M, neither of which, however, occurs in the bulk. Here we demonstrate from a combination of first-principles calculations, group-theoretic techniques, and spin models that this structural trimerization not only exists in a family of hexagonal $RFeO_3$ ferrites, but also induces a bulk M, leading to a bulk coupling of ferroelectric and ferromagnetic domains such that if the polarization, P, reverses so does M. We show how this trimer distortion mediates an trilinear-coupling of P, M, and antiferromagnetic order, which is a universal feature of the hexagonal ferrites.

arXiv:1302.1099v1 [cond-mat.mtrl-sci] 5 Feb 2013

Two themes at the forefront of materials physics are the cross-coupling of distinct types of ferroic order [1–4] and topological defects in systems with spontaneous broken symmetry [5–8]. Common to both are a plethora of novel phenomena to understand, and new properties and functionalities to exploit for novel applications. Multiferroics [9, 10] are an ideal platform to realize both themes in a single material. In this regard, an exciting development is the discovery of a topologically protected vortex-domain structure in one of the most extensively studied class of multiferroics, the hexagonal (hexa) rare-earth manganites. Here, antiphase structural ('trimer') domains are clamped to ferroelectric domain walls (and vice versa) [11–14] forming a 'clover-leaf' domain pattern, Fig. 1a. These trimer domains have a particular phase relationship that lead to an appearance of structural vortices, which in turn induce magnetic vortices [15, 16], strongly coupling antiferromagnetism and the polarization at the domain wall. This leads to a significant domain wall magnetoelectric effect and magnetization neither of which, however, occurs in the bulk.

Our focus here is on elucidating a remarkable family of materials, the hexa $RFeO_3$ ferrites. We show they display all the ingredients necessary to realize the vortex-domain physics plus an intrinsic, bulk magnetization, $\mathbf{M}$, induced by the trimer distortion, $\mathbf{Q}^{\Psi}_{K_3}$, leading to entirely new magnetoelectric phenomena absent in manganites.

The crystal structure of the hexa manganites is formed by a two-dimensional network of corner shared trigonal MnO_5 bipyramids, separated by layers of R ions, Fig. 1b. Geometric frustration of the strongly antiferromagnetic, AFM, nearest neighbor Mn spins leads to 120° non-collinear AFM ordering ($T_N \approx$ 80-120 K). The key to realizing the unusual topological defects and strong coupling at the domain walls is the improper nature of ferroelectricity in this class of materials. Here the polarization, $\mathbf{P}$, which is stable in the paraelectric $P6_3/mmc$ structure, is induced by a zone-tripling structural distortion, $\mathbf{Q}^{\Psi}_{K_3}$ [16–18]. The latter, referred to as the trimer distortion, is associated with a 2-up/1-down buckling of the R-planes and tilting of the MnO_5 bypyramids. It is nonlinearly coupled to the polarization,

$$\mathcal{F}_{\rm trimer} \sim P Q^3_{K_3} \cos(3\Psi) \qquad (1)$$

the form of which implies that a nonzero trimer distortion induces a nonzero $\mathbf{P}$. There are three distinct Ψ domains (α, β, and γ) corresponding to one of three possible $\tilde{2}_c$ axes, i.e., one of the 3 permutations of 2-up/1-down. Also there are two tilting directions, either towards (+) or away from (−) the $\tilde{2}_c$ axis, i.e., 1-up/2-down or 2-up/1-down, respectively. This results in six $P6_3cm$ structural domains. A consequence of the improper origin of ferroelectricity is that the sign of $\mathbf{P}$ depends on the direction of $\mathbf{Q}^{\Psi}_{K_3}$. This simple fact leads to the nontrivial domain structure of the hexa manganites, Fig 1a [11–13, 16].

Recently thin films of $RFeO_3$ have been epitaxially stabilized in the hexa $P6_3cm$ structure [19, 20]. These hexa ferrites exhibit ferroelectricity above room temperature, but with conflicting results as to its origin [21, 22]. As to the magnetic structure, experiments on $LuFeO_3$ suggest a considerably high AFM ordering temperature, T_N = 440 K [23]. Additionally there is evidence of a second magnetic transition around ∼ 100K, at which $\mathbf{M}$ becomes nonzero [21–24], however, the significance of this or even if it is an intrinsic or bulk effect is not previously known.

Our main results are as follows: 1) ferroelectricity in the hexa ferrites is of the improper structural type where the trimer distortion induces $\mathbf{P}$, and therefore a similar topological domain structure exists as in the manganites, however, the difference in electronic structure leads to 2) Fe spins ordering above room temperature and to 3) an 120° AFM structure, $\mathbf{L}$, that allows weak-ferromagnetism ($M||z$) induced by $\mathbf{Q}^{\Psi}_{K_3}$. The combined significance of which 4) suggests a bulk coupling of trimer/ferroelectric, FE, and ferromagnetic, FM, domains such that if $\mathbf{P}$ reverses 180° so does $\mathbf{M}$. A universal feature of all hexa ferrites is that the trimer distortion induces both $\mathbf{P}$ and $\mathbf{M}$, and mediates an intrinsic bulk coupling of $\mathbf{P}$, $\mathbf{M}$, and $\mathbf{L}$. These results are summarized in Figs. 1c-e. In the remainder of this paper we explain these results and discuss the novel implications for the topological domain structure.

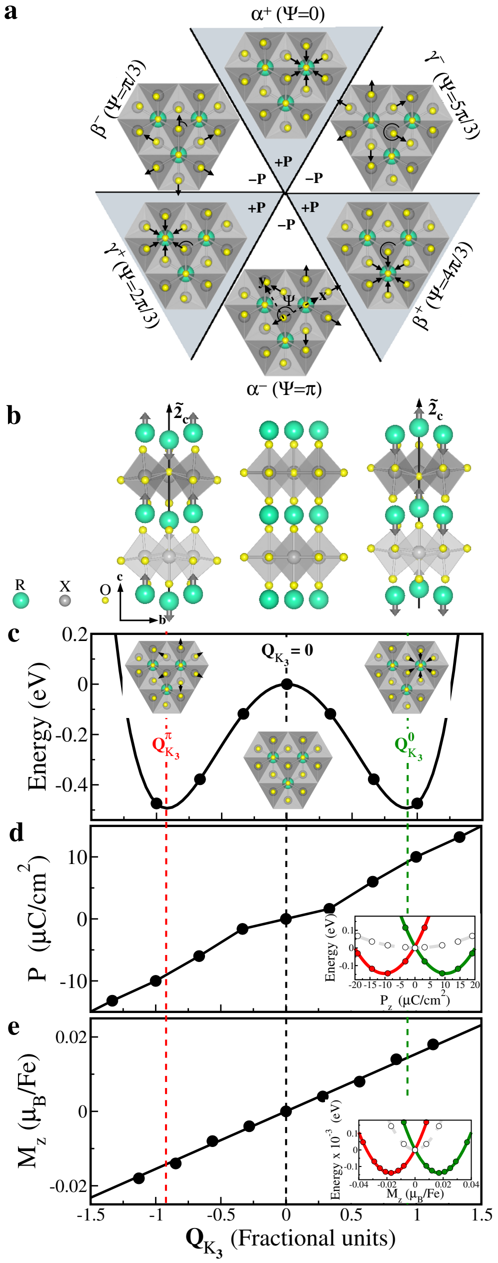

FIG. 1. **Improper structural ferroelectricity inducing weak-ferromagnetism, $\mathbf{M}_z$, in hexagonal ferrites from first principles.** Results are shown for $LuFeO_3$ but (a-d) hold for $RFeO_3$ and $RMnO_3$, while (e) occurs only for ferrites. **a**, Six structural domains of the primary "trimer" $\mathbf{Q}^{\Psi}_{K_3}$ distortion and the secondary polarization $\mathbf{P}$ where $P \sim Q^3_{K_3}\cos 3\Psi$. Here $\alpha^+ \iff \Psi = 0$ and a counterclockwise rotation corresponds to domains differing by $\Psi = +\pi/3$. Arrows indicate the direction of the trimer distortions, only distortions around the $\tilde{2}_c$ axis are shown for clarity. **b**, Crystal structure of the (left) $\mathbf{Q}^{\pi}_{K_3} = -Q_{K_3}$ (α^-), (center) paraelectric $Q_{K_3} = 0$, and (right) $\mathbf{Q}^{0}_{K_3} = +Q_{K_3}$ (α^+), domains respectively. **c**, Energy, **d**, **P**, and **e**, $\mathbf{M}_z$ as a function of Q_{K_3}, allowing only $\Psi = 0$ or π trimer domains. Notice that $\mathbf{P}$ =0 when $\mathbf{Q}^{\Psi}_{K_3} = 0$, suggesting that a proper ferroelectric mechanism in not likely (see Supplemental). The insets of **d**, and **e**, show Energy vs. **P** and $\mathbf{M}_z$, respectively.

Route to elucidate cross coupling of bulk order. Our approach to elucidate the bulk cross-coupling between ferroelectricity and magnetism is to introduce a $P6_3/mmc$ paraelectric, PE, reference structure that has the same AFM configuration as the $P6_3cm$ FE ground state. The minimal model required to describe the spin structure [25] is the following effective spin Hamiltonian

$$H = \sum_{ij} J_{ij}\mathbf{S}_i\cdot\mathbf{S}_j + \sum_{ij}\mathbf{D}_{ij}\cdot\mathbf{S}_j\times\mathbf{S}_j + \sum_i \mathbf{S}_i\cdot\hat{\boldsymbol{\Phi}}_i\cdot\mathbf{S}_i \quad (2)$$

where the J_{ij}'s are the symmetric exchange interactions, D_{ij}'s are the Dzyaloshinskii-Moriya (DM) antisymmetric exchange vectors, and $\hat{\boldsymbol{\Phi}}_i$ is the single-ion anisotropy (SIA) tensor. Using this model as a guide, we then calculate from first principles how the material specific parameters of this model change on going from the PE reference structure to the FE ground state as a function of the trimer distortion. This also will allow us to explain why manganites and ferrites have qualitatively different magnetic order. Additionally, we will introduce a simple phenomenological model that captures the essential physics, explaining our first-principles results and providing an intuitive rational for the spin model.

Method. The first principles calculations were performed using the DFT+U method [26] with the PBE form of exchange correlation functional [27]. We considered Lu $4f$ states in the core and for TM $3d$ states we chose U = 4.5 eV and J_H = 0.95 eV. Structural relaxations, frozen phonon and electric polarization calculations were performed without the spin-orbit coupling (SOC) using the projected augmented plane-wave basis based method as implemented in the VASP [28, 29]. We used a 4×4×2 k-point mesh and a kinetic energy cut-off of 500 eV. The Hellman-Feynman forces were converged to 0.001 eV/Å. The electronic and magnetic properties were studied in the presence of SOC.

We additionally cross-validated the electronic and magnetic properties using the Full-potential Linear Augmented Plane Wave (FLAPW) method as implemented in WIEN2K code [30].

The magnetic ground state. In the PE structure the transition metal, TM, spins form ideal triangular planes, which become slightly distorted in the FE phase. If the in-plane nearest neighbor (nn) TM-TM exchange interactions are AFM in nature, geometric frustration would cause the spins to order in a 120° non-collinear pattern, as in the manganites. Considering the compatibility of this spin pattern with that of the crystal symmetry, four principle 120° magnetic spin configurations, denoted A_1, A_2, B_1 and B_2, are allowed, Fig. 2a. Among these four principle phases only A_2 (magnetic space group $P6_3c'm'$) allows a net $\mathbf{M}$ along $\hat{z}$. These spin states are defined by two free parameters, χ_1 and χ_2, as described in Fig. 2a.

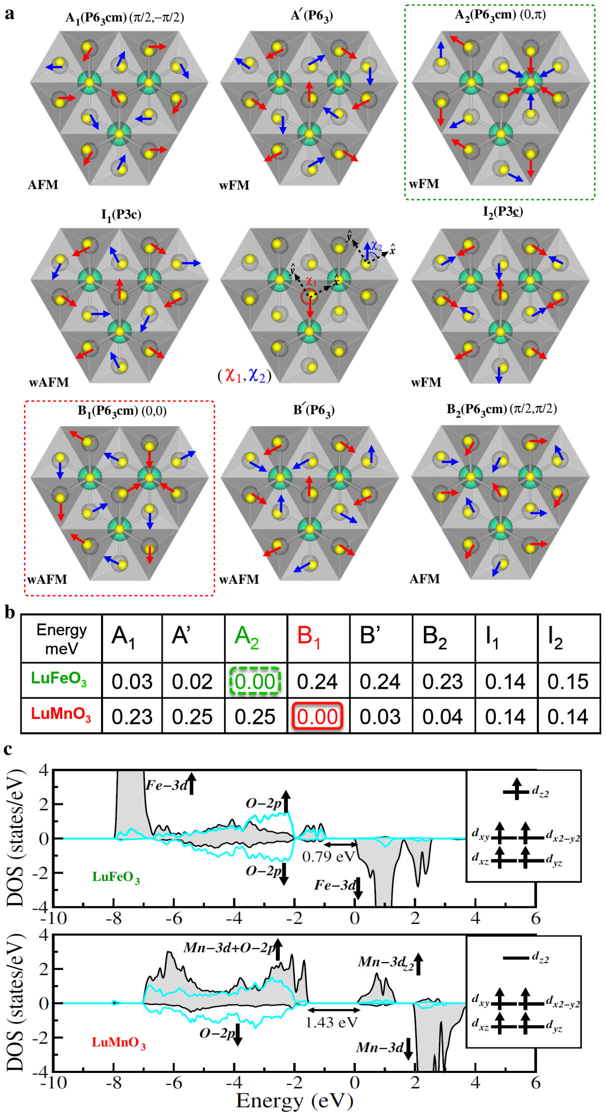

Energy meV	A_1	A'	A_2	B_1	B'	B_2	I_1	I_2
$LuFeO_3$	0.03	0.02	0.00	0.24	0.24	0.23	0.14	0.15
$LuMnO_3$	0.23	0.25	0.25	0.00	0.03	0.04	0.14	0.14

FIG. 2. **The noncollinear magnetic and electronic structure from first principles.** **a**, The 120° antiferromagnetic (AFM) ordering patterns – arrows indicate the spin direction within the xy plane. For each bipyramid layer, $\alpha = \mathbf{1}$ (red arrows, darker triangles) or $\mathbf{2}$ (blue arrows, lighter triangles), we define a local AFM order parameter, $L_\alpha = L_{xy}e^{i\chi_\alpha}$. The values of the angles (χ_1,χ_2), shown for the $\Psi = 0$ trimer domain, are defined by specific TM ions from adjacent planes connected by the $\tilde{2}_c$ axis that remains in the distorted phase. Among the four principle magnetic structures only A_2 and B_1 allow the xy spins to uniformly cant out of plane resulting in a net layer magnetization, $\mathbf{M}^z_\alpha = M^z_\alpha\hat{z}$, and to weak-ferromagnetism (wFM) or weak-antiferromagnetism (wAFM), respectively. All intermediate spin patterns can be described as a linear combination of the four principle magnetic structures. First-principles calculations of **b**, Noncollinear magnetic energies and **c**, density of states (collinear). Note that the difference in orbital occupancy is the fundamental reason why ferrites, top, and manganites, bottom, have different magnetic ground states and subsequently the key to the predicted bulk coupling of polarization and magnetism in ferrites. Insets: crystal field splitting and occupancy of the TM majority $3d$ channel.

In addition to the principle magnetic configurations we also considered the four known intermediate magnetic structures, Fig. 2a. The results of our total energy calculations for $LuFeO_3$, LFO, and $LuMnO_3$, LMO, are presented in Fig. 2b (for clarity we limit our discussion to these two compounds). In agreement with non-linear optical measurements [31], we find that LMO stabilizes in the B_1 state. Interestingly, this state displays weak-antiferromagentism, wAFM, i.e., there is a small canting of the spins out of the xy-plane, which leads to a net moment in each layer but consecutive layers cant in opposite directions leading to a net $\mathbf{M}_z = 0$. Note, however, that the B_2 state, where the net magnetic moment is equal to zero in each layer by symmetry, is also close in energy.

In contrast, LFO stabilizes in the A_2 state where a canting of the spins out of the xy-plane is also allowed but here consecutive layers add, leading to a net $\mathbf{M}_z = 0.02\mu_B$/Fe along the z-axis, i.e., LFO displays weak-ferromagnetism, wFM [32, 33]. As shown in Fig. 2b, however, the A_1 ($\mathbf{M}_z = 0$ by symmetry) and A' (finite $\mathbf{M}_z$ allowed) states, lie energetically very close to ground state. It was recently inferred from neutron diffraction [23] that LFO orders above room temperature (high for a frustrated magnet) in an AFM state with $\mathbf{M}_z = 0$, and at a lower temperature undergoes a reorientation transition to the A' phase inducing a $\mathbf{M}_z \neq 0$. Our calculations do support such a picture, however, we emphasize that this wFM state (A' can be thought of as a linear combination of A_1 and A_2) is far more unusual than what could have been anticipated.

The electronic ground state. In the PE phase the crystal field at the TM site has a D_{3h} trigonal point symmetry, which splits atomic $3d$ levels into three sets of states as shown in the insets of Fig.2c. In the order of increasing energy these are: e' doublet composed of d_{xz} and d_{yz} states, e'' doublet composed of d_{xy} and $d_{x^2-y^2}$states, and a'_1 singlet that corresponds to d_{3z^2} state. It is convenient to adopt this notation also in the low-temperature phase, even though in this case the crystal field has lower symmetry and the doublets split into singlets. The density of states (DOS) plots calculated for LFO and LMO in the FE phase are shown in Fig. 2c. LFO is a charge-transfer insulator with the conduction band formed by minority Fe $3d$ states and the valence band composed of O $2p$ states, below which are the filled majority Fe $3d$ bands. In the case of LMO majority $3d$ bands are partially filled with occupied e' and e''. Due to smaller nuclear charge of Mn these bands lie at higher energies as compared to LFO and they overlap with O $2p$ states forming the valence band. At the conduction band minimum we have the empty majority a'_1 states while minority $3d$ levels lie at somehow higher energies. The importance of these differences will be made clear when discussing the magnetic interactions.

Symmetric exchange. There are two important symmetric exchange interactions. The first is a strong, AFM superexchange interaction between in-plane nn spins, J_{nn}. Its magnitude is much larger for LFO compared with LMO, suggesting a substantially larger magnetic ordering temperature for ferrites (within mean field theory the calculated Currie-Weiss temperature for LFO in the FE phase is $\Theta_{CW} = 1525$ K, while in LMO $\Theta_{CW} = 274$ K [34]).

The second is a weak, super-superexchange interaction, J_c, which couples consecutive spin planes via a TM-O-Lu-O-TM exchange pathway. In the PE structure, a spin in one layer is connected to three spins in a consecutive layer. Each of these degenerate spin-spin interactions has two equivalent exchange pathways. We find that the interlayer exchange is AFM for LFO but FM for LMO. Although the strength of this interaction is relatively weak, this sign difference turns out to be key.

In the PE structure symmetry implies that the relative orientation of the spins in consecutive spin planes is arbitrary. The trimer distortion, however, splits the three degenerate interactions into: a single J_c^{11} interaction, mediated by two equivalent TM-O-Lu1-O-TM exchange pathways, and two J_c^{12} interactions, where each interaction is mediated by a TM-O-Lu1-O-TM and a TM-O-Lu2-O-TM exchange pathway. This remarkably introduces an extra contribution to the energy

$$E_{\text{intra}}^{\text{SE}} = 2\Delta J_c \cos(\chi_1 - \chi_2) \tag{3}$$

where $\Delta J_c = J_c^{11} - J_c^{12}$, for which the sign is key in determining the magnetic configuration type: A-type ($\chi_2 = \chi_1 + \pi$) for $\Delta J_c > 0$ or B-type ($\chi_2 = \chi_1$) for $\Delta J_c < 0$.

A simple structural analysis shows that the super-super exchange mediated through the Lu_2 ion is always weaker than that mediated through the Lu_1 ion, and indeed our calculations show that the magnitude of J_c^{11} is always larger than J_c^{12}. We therefore see that the choice between A-type and B-type in the FE structure is in fact determined by the sign of J_c in the PE structure. This is important. In ferrites, the AFM nature of the interlayer exchange is uniquely determined by the orbital occupancy, it is always AFM and therefore ferrites will always prefer *A*-type magnetic configurations and the wFM ground state. (Although the interlayer exchange in LMO is FM, which explains why it prefers *B*-type magnetic configurations, it is not universally so; a discussion is given in the Supplement).

Dzyaloshinskii-Moriya and Anisotropy. Symmetric exchange determines the magnetic configuration type. It is the DM interactions and SIA that drives spin canting. (Note, our calculations reveal that a dominant DM interaction, $\mathbf{D}_{ij}$, exists only between nn spins within the triangular planes.) Let us first consider the PE structure. Here the DM vector has only a $\hat{z}$ component, which favors spin ordering within the xy plane while the SIA tensor is diagonal with only one independent parameter, Φ^{zz}. In the FE structure, however, the trimer distortion *induces* both a transverse component of the DM vector, $\mathbf{D}_{ij}^{xy}$, parallel to the xy plane and an off-diagonal component to the SIA tensor, Φ_{xz} [35].

These trimer-induced interactions lead to a further energy lowering if the spins in each layer, α, cant out of their respective xy plane. The canting angle in each layer is determined by minimizing Eq. 2 and is found to be

$$M_\alpha^z \propto \tan(2\theta_\alpha) \approx \frac{(2\sqrt{3}D_{xy} - \Phi_{xz})\cos(\chi_\alpha)}{3J_{nn}}, \tag{4}$$

for the $\Psi = 0$ domain, which vanishes in the PE phase (as $D_{xy} \propto \Phi_{xz} \propto Q_{K_3} = 0$, where $D_{xy} \equiv |\mathbf{D}_{ij}^{xy}|$).

Note that this result is easily generalizable to any Ψ-domain. Next we consider a simple phenomenological model that provides a more intuitive interpretation and rigorous generalization of these spin model results and will clearly show that *the trimer-induced exchange interactions are responsible for the bulk* **P-M** *coupling.*

The phenomenological model. The crystallographic structure suggests that insight may be gained by considering order parameters, OPs, local to each of the two bipyramid layers. Within each layer, α, a local magnetic structure can be defined as a combination of 120° AFM order in the $\hat{x}\hat{y}$ plane, $L_\alpha = L_{xy}e^{i\chi_\alpha}$, and a net magnetization along $\hat{z}$, M_α^z. A specific choice of angles (χ_1,χ_2), which are defined by specific TM ions from adjacent triangular planes connected by the $\tilde{2}_c$ axis that remains in the FE phase, describes any possible AFM spin pattern shown in Fig. 2a. Additionally there are two ways to combine the layer magnetizations: $M_z \equiv M_1^z + M_2^z$ and $L_z \equiv M_1^z - M_2^z$.

Following a similar line of reasoning, we describe the total trimer distortion, $\mathbf{Q}_{K_3}^{\Psi}$, as the sum of two local ones, $Q_\alpha = Q_{K_3}e^{i\Psi_\alpha}$, where we generalize the suggestion by Artyukhin et al., [16] and define Ψ_α as the angle that describes the in-plane displacement of the apical oxygen that lies directly above the reference spin, L_α, as shown in Fig. 3a. Note that $\Psi_1 = \pi - \Psi_2 \equiv \Psi$ is fixed by the symmetry of the trimer distortion, therefore specific Ψ_α's are associated with the different trimer domains, Fig. 1a.

Let us ask the question, when is a (local) trilinear coupling between Q_α, L_α, and either M_z or L_z allowed by the symmetry of the AFM-PE reference structure. A derivation is provided in the Supplemental but note, only invariants that contain $\Re[X_\eta]$ ($\Re \equiv$ real part), where $X_\eta \equiv Q_1L_1^* + \eta Q_2L_2^*$ and $\eta = \pm$ (e.g., pairs like $Q_\alpha\ L_\alpha^*$ are required to preserve translational symmetry), can be formed. We find two allowed couplings,

$$F_{\text{tri}}^{M} \sim \Re[X_+]M_z = (\mathbf{Q}_1 \cdot \mathbf{L}_1 + \mathbf{Q}_2 \cdot \mathbf{L}_2)M_z \tag{5}$$

$$F_{\text{tri}}^{L_z} \sim \Re[X_-]L_z = (\mathbf{Q}_1 \cdot \mathbf{L}_1 - \mathbf{Q}_2 \cdot \mathbf{L}_2)L_z \tag{6}$$

with $\mathbf{L}_\alpha \equiv L_{xy}(\hat{x}\cos\chi_\alpha + \hat{y}\sin\chi_\alpha)$ and $\mathbf{Q}_\alpha \equiv Q_{K_3}(\hat{x}\cos\Psi_\alpha + \hat{y}\sin\Psi_\alpha)$. The presence of either invariant indicates that as the system enters the FE phase, the trimer distortion induces a canting of the AFM ordered spins in each plane, leading to a trimer-induced wFM or

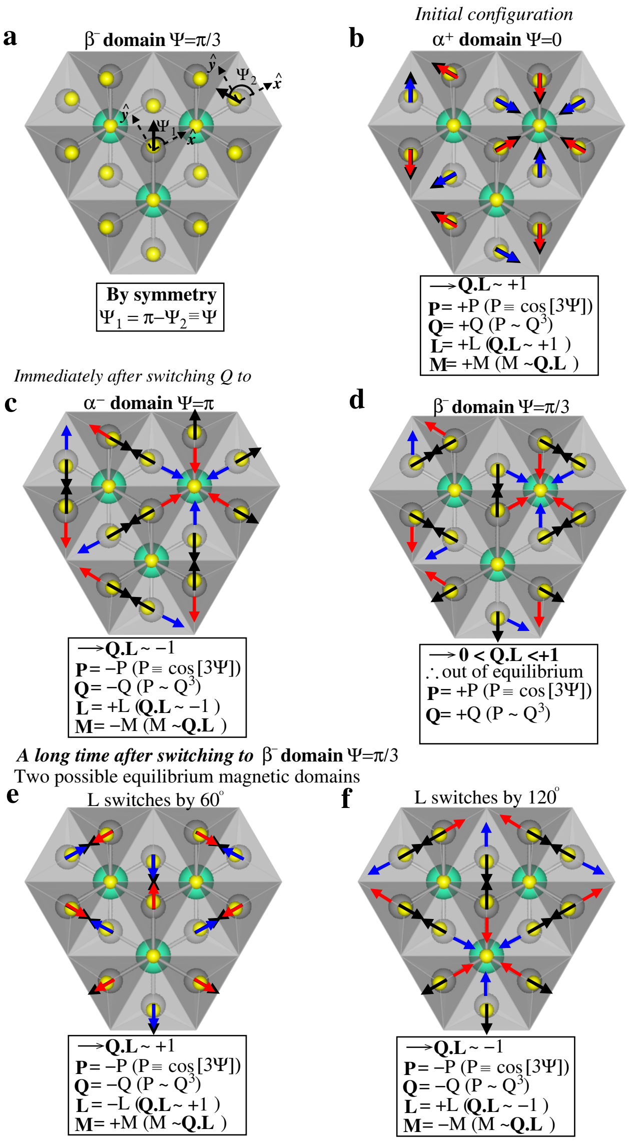

FIG. 3. **Bulk cross-coupling of polarization and magnetization in hexagonal ferrites.** Thought experiment to elucidate the cross-coupling of ferroelectricity and magnetism mediated by the trimer distortion for the predicted A_2 magnetic ground state. **a,** Definition of local trimer angles Ψ_1 and Ψ_2, **b,** Initial equilibrium α^+ domain $\equiv$ {+P,+Q, +L_{xy}, +M_z}. Immediately after switching **c,** to the α^- domain, L_{xy} still in ground state, therefore +M_z → -M_z; α^- domain $\equiv$ {-P,-Q, +L_{xy}, -M_z}, **d,** β^- domain, L_{xy} is not in a ground state and must rotate either, **e,** 60°, therefore +M_z → +M_z; β^- domain $\equiv$ {-P,-Q, -L_{xy}, +M_z}, or **f,** 120°, therefore +M_z → -M_z; β^- domain $\equiv$ {-P,-Q, +L_{xy}, -M_z}.

wAFM, respectively [36]. Notice that Eq. 5 not only contains the spin model result, Eq. 4, but also generalizes it to any Ψ-domain. This connection can be made more apparent by defining $\mathbf{D}_\alpha$ by $\mathbf{Q}_\alpha = \hat{\mathbf{z}} \times \mathbf{D}_\alpha$, then

$$F^{M}_{tri} \sim [\mathbf{D}_1 \cdot (\mathbf{L}_1 \times \hat{\mathbf{z}}) + \mathbf{D}_2 \cdot (\mathbf{L}_2 \times \hat{\mathbf{z}})] M_z \qquad (7)$$

$$F^{L_z}_{tri} \sim [\mathbf{D}_1 \cdot (\mathbf{L}_1 \times \hat{\mathbf{z}}) - \mathbf{D}_2 \cdot (\mathbf{L}_2 \times \hat{\mathbf{z}})] L_z \qquad (8)$$

leading to an induced magnetization, $\mathbf{M}^z_\alpha \propto (\mathbf{D}_\alpha \times \mathbf{L}_\alpha)$. We interpret $\mathbf{D}_\alpha$ as an effective transverse DM vector, $\mathbf{D}^{xy}_\alpha$, for each layer that is induced by the local trimer distortion (this can be derived, see Supplemental).

We see that writing in terms of local OPs has several conceptual advantages. First, it is immediately clear that in the FE phase canting occurs only when there is a nonzero projection of an xy-spin along the direction of the local trimer distortion, i.e., $M^z_\alpha \propto \mathbf{Q}_\alpha \cdot \mathbf{L}_\alpha$. This is why there is no canting for the A_1 and B_2 spin configurations, as the local spins are perpendicular to the local trimer distortions. In the A_2 and B_1 configurations, however, the local $\hat{xy}$-spins and trimer distortions are parallel (or antiparallel), where the only difference being that in the A_2 state this projection has the same sign in adjacent layers while in the B_1 state the projection changes sign, resulting in a nonzero F^{M}_{tri} and $F^{L_z}_{\mathrm{tri}}$, respectively. Since an intermediate spin state can be thought of as a linear combination of principle spin structures, any one with a nonzero A_2 (B_1) component will exhibit wFM (wAFM).

Implications of the trilinear coupling. The trilinear coupling of Eq. 5 is quite remarkable. It implies that in ferrites the trimer distortion not only induces a polarization, Eq. 1, but also mediates a non-trivial bulk **P**-**M** coupling. To make this clear, we consider a thought experiment in which an applied electric field, $\vec{E}$, can switch **P** to any one of the three trimer domains with −**P** (more in the Discussion). Let the system be initially in the α^+ domain, Fig. 3b, with $\mathbf{P} = +\mathrm{P}$ and $\mathbf{Q}_\alpha \cdot \mathbf{L}_\alpha = +1$, apply $\vec{E}$ and consider two cases:

$\{\alpha^+ \rightarrow \alpha^-\}$. In a proper FE like $\mathrm{PbTiO_3}$ the structure of the +**P** domain is related to the −**P** domain by a reversal in the direction of the polar distortions *w.r.t* the PE structure, e.g, the $\mathrm{Ti^{4+}}$ ion moving from up to down. The analogous situation in the hexa systems corresponds to a structural change from a 2-up/1-down buckling and tilting ‘out’ of the R-planes and bypyramids, respectively, to a 1-up/2-down and tilting ‘in’, while remaining in the same distinct domain, e.g., α. This corresponds to switching **P** via rotating Ψ by π. In this α^- domain $\mathbf{Q}_\alpha \cdot \mathbf{L}_\alpha = -1$, Fig. 3c, and therefore, because of Eq. 5, either L_α has to rotate 180° or the small canting angle has to change sign. It is not unreasonable to expect the latter to be more favorable, leading to a reversal of $\mathbf{M}_z$. This is the scenario previously discussed in Fig. 1.

$\{\alpha^+ \rightarrow \beta^-\}$. The improper nature of ferroelectricity, however, offers an even more interesting possibility in that there exists three distinct and accessible domains (α, β, and γ). As an example let **P** switch via rotating Ψ by π/3 and consider the configuration immediately after, Fig. 3d. In this β^- domain $0 < \mathbf{Q}_\alpha \cdot \mathbf{L}_\alpha < +1$, implying the system is not in equilibrium, and therefore L_α must rotate by either π/3, Fig. 3e, or −2π/3, Fig. 3f. In the former case $\mathbf{Q}_\alpha \cdot \mathbf{L}_\alpha = +1$ as in the initial α^+ configuration, therefore $\mathbf{M}_z$ is not reversed, while in the latter

$\mathbf{Q}_\alpha \cdot \mathbf{L}_\alpha = -1$ and $\mathbf{M}_z$ switches 180°.

Discussion. In this paper we have discussed an intriguing family of improper ferroelectrics where we have shown for the first time that a non-polar trimer structural distortion not only induces an electrical polarization but also induces weak-ferromagnetism. It is a universal feature of these hexa ferrites systems that they stabilize in one of the A-type states, all of which (except for one, the A_1 state) allow for a weak ferromagnetic moment along $\hat{z}$. Due to a competition between spin canting and in-plane anisotropy, the magnetic ground state is the A_2 magnetic phase. It is important to note that exchange interactions in these ferrites are much larger compared with the manganites, which indicates the possibility for a much higher magnetic transition temperature and an above room temperature multiferroic, the observation of which has been recently suggested by [23].

Here, however, we discussed a result even more exciting – the trimer distortion mediating an intrinsic bulk trilinear-coupling of the polarization, magnetization, and antiferromagnetic order. Due to the improper nature of ferroelectricity, the topologically protected trimer domains have a particular phase relationship that leads to an appearance of structural vortices, which in turn induce magnetic vortices [16]. In these ferrites we additionally have the nontrivial bulk magnetoelectric effect, and it is natural to ask what type of domains would one expect to see here? Here we dsicuss two likely domain patterns, Fig. 4, but by no means is this meant to be exhaustive. Both assume that the only AFM domain walls are those clamped to the trimer domain walls [16].

The first domain configuration, Fig. 4a, is such that at trimer domain walls differing by $\Delta\Psi = \pi/3$, e.g., at the α^+ and β^- domain wall, the AFM spins rotate $\Delta\chi_\alpha = |\pi/3|$. In this case the direction of the magnetization remains the same across the domain wall as we previously explained in Fig. 3e. Note that this seemingly lower energy AFM switching pathway results in a homogeneous magnetization across the entire material, which has to be unstable towards the formation of ferromagnetic domains. But what kind of domains? In these hexa systems $\pm\mathbf{M}_z$ domains result from the reorientation of the $\mathbf{L}_{xy}$ vector by an angle π. They can occur within the bulk of a trimer domain, i.e., a free AFM domain, but there is an energy cost to form the domain wall.

An alternative path to minimize the total energy of the system is considered in Fig. 4b, where at trimer domain walls that differ by $\Delta\Psi = \pi/3$ the AFM spins now rotate $\Delta\chi_\alpha = |2\pi/3|$. In this case, the magnetization direction reverses with the polarization as discussed in Fig. 3f. Therefore, even though this domain configuration at first appears less likely than Fig 4a, it provides an avenue for the system to minimize the magnetostatic energy without having to introduce free domains.

Finally, the hexa ferrites provide an intriguing route to a bulk magnetoelectric effect and electric-field control over the direction of the magnetization. In Fig. 4c we sketch the expected response of the domains to electric-field poling. (Note that as the domain walls are topologically protected, however, -P domains do not disappear completely [11, 16].) In this process the positive electric field, E, e.g., choses the (+P,+M) state and therefore reversing of the direction of electric field will not only switch the direction of polarization, but also reverses the direction of magnetization.

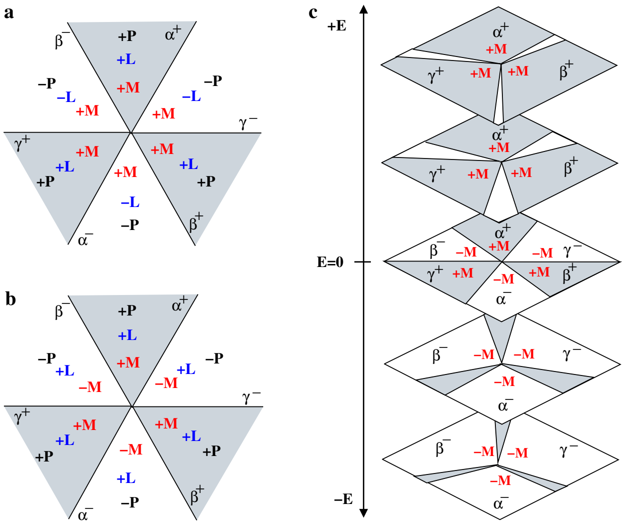

FIG. 4. **Clamping of trimer and magnetic domains and electric field response.** At the lowest energy trimer domain wall Ψ changes by $\pi/3$, which will rotate the AFM order parameter L_1 and L_2 by either **a**, $\pi/3$ and $-\pi/3$ or **b**, $-2\pi/3$ and $2\pi/3$. In the former case $\mathbf{M}_z$ remains constant while in the latter $\mathbf{M}_z$ reverese at each trimer domain wall, i.e., ferroelectric, ferromagnetic, and trimer domains are mutually clamped. **c**, The schematic diagram displaying the electric-field switching of ferromagnetic domains (note, the figure is inspired by Ref.[11])

Acknowledgments

We acknowledge discussions with D.G. Schlom, P. Schiffer and J.Moyer. This work started at the suggestion of D.G.S. HD was supported by the DOE-BES under Award Number de-sc0005032. AW was supported by the Cornell Center for Materials Research with funding from NSF MRSEC program, cooperative agreement DMR-1120296. CJF was supported by the DOE-BES under Award Number DE-SCOO02334.

[1] E. Bousquet, M. Dawber, N. Stucki, C. Lichtensteiger, P. Hermet, S. Gariglio, J.-M. Triscone, and Ph. Ghosez, Nature **452**, 732 (2008).

[2] Y. Tokunaga, N. Furukawa, H. Sakai, Y. Taguchi, T.-h.

Arima, and Y. Tokura, Nat Mater **8**, 558 (2009).

[3] J. H. Lee, L. Fang, E. Vlahos, X. Ke, Y. W. Jung, L. F. Kourkoutis, J.-W. Kim, P. J. Ryan, T. Heeg, M. Roeckerath, et al., Nature **466**, 954 (2010).

[4] Y. Tokunaga, Y. Taguchi, T.-h. Arima, and Y. Tokura, Nat Phys **8**, 838 (2012).

[5] N. D. Mermin, Rev. Mod. Phys. **51**, 591 (1979).

[6] N. Balke, B. Winchester, W. Ren, Y. H. Chu, A. N. Morozovska, E. A. Eliseev, M. Huijben, R. K. Vasudevan, P. Maksymovych, J. Britson, et al., Nat Phys **8**, 81 (2012).

[7] D. Meier, J. Seidel, A. Cano, K. Delaney, Y. Kumagai, M. Mostovoy, N. A. Spaldin, R. Ramesh, and M. Fiebig, Nature Materials **11**, 284 (2012).

[8] A. K. Tagantsev and E. B. Sonin, Ferroelectrics **98**, 297 (1989).

[9] R. Ramesh and N. A. Spaldin, Nat Mater **6**, 21 (2007).

[10] S.-W. Cheong and M. Mostovoy, Nat Mater **6**, 13 (2007).

[11] T. Choi, Y. Horibe, H. T. Yi, Y. J. Choi, W. Wu, and S. W. Cheong, Nat Mater **9**, 253 (2010).

[12] S. C. Chae, Y. Horibe, D. Y. Jeong, S. Rodan, N. Lee, and S. W. Cheong, Proceedings of the National Academy of Sciences **107**, 21366 (2010).

[13] M. Mostovoy, Nat Mater **9**, 188 (2010).

[14] Y. Kumagai and N. A. Spaldin, ArXiv e-prints (2012), 1207.4080.

[15] Y. Geng, N. Lee, Y. J. Choi, S.-W. Cheong, and W. Wu, Nano Letters **12**, 6055 (2012).

[16] S. Artyukhin, K. T. Delaney, N. A. Spaldin, and M. Mostovoy, ArXiv e-prints (2012), 1204.4126.

[17] B. B. Van Aken, T. T. M. Palstra, A. Filippetti, and N. A. Spaldin, Nat Mater **3**, 164 (2004).

[18] C. J. Fennie and K. M. Rabe, Phys. Rev. B **72**, 100103 (2005).

[19] A. A. Bossak, I. E. Graboy, O. Y. Gorbenko, A. R. Kaul, M. S. Kartavtseva, V. L. Svetchnikov, and H. W. Zandbergen, Chemistry of Materials **16**, 1751 (2004).

[20] E. Magome, C. Moriyoshi, Y. Kuroiwa, A. Masuno, and H. Inoue, Japanese Journal of Applied Physics **49**, 09ME06 (2010).

[21] Y. K. Jeong, J.-H. Lee, S.-J. Ahn, and H. M. Jang, Chemistry of Materials **24**, 2426 (2012).

[22] Y. K. Jeong, J.-H. Lee, S.-J. Ahn, S.-W. Song, H. M. Jang, H. Choi, and J. F. Scott, Journal of the American Chemical Society **134**, 1450 (2012).

[23] W. Wang, J. Zhao, Z. Gai, N. Balke, M. Chi, H. N. Lee, W. Tian, L. Zhu, X. Cheng, D. J. Keavney, et al., ArXiv e-prints (2012), 1209.3293.

[24] A. R. Akbashev, A. S. Semisalova, N. S. Perov, and A. R. Kaul, Applied Physics Letters **99**, 122502 (pages 3) (2011).

[25] I. V. Solovyev, M. V. Valentyuk, and V. V. Mazurenko, Phys. Rev. B **86**, 054407 (2012).

[26] V. I. Anisimov, F. Aryasetiawan, and A. I. Lichtenstein, Journal of Physics: Condensed Matter **9**, 767 (1997).

[27] J. P. Perdew, K. Burke, and M. Ernzerhof, Phys. Rev. Lett. **77**, 3865 (1996).

[28] Kresse, G. and Hafner, J. , Phys. Rev. B **47**, 558 (1993).

[29] Kresse, G. and Furthmüller, J. , Phys. Rev. B **54**, 11169 (1996).

[30] P. Blaha, K. Schwartz, G. K. H. Madsen, D. Kvasnicka, and J. Luitz, wIEN2K, An Augmented Plane Wave + Local Orbitals Program for Calculating Crystal Properties, edited by K. Schwarz (Technische Universitatâ Wien, Vienna, 2001).

[31] M. Fiebig, D. Fröhlich, K. Kohn, S. Leute, T. Lottermoser, V. V. Pavlov, and R. V. Pisarev, Phys. Rev. Lett. **84**, 5620 (2000).

[32] I. E. Dzyaloshinskii, Sov. Phys. JETP **5**, 1259 (1957).

[33] T. Moriya, Phys. Rev. **120**, 91 (1960).

[34] For LMO Θ_{CW} is strongly underestimated as compared with experimental value of 510 K. This indicates that the value of $U = 4.5$ eV is too large for LMO. Repeating the calculations for smaller values U we reached a reasonable agreement with experiment for $U = 2$ eV.

[35] Additionally, an in-plane anisotropy, $\Phi_{xx} \neq \Phi_{yy} \propto \sin^2 \alpha$, where $\alpha \propto Q_{K_3} \sim 5^\circ$ is the tilting angle of the bipyramids associated with the trimer distortion, is induced but very small. In contrast, the *induced* off-diagonal SIA can be and is substantially larger as seen in Table 1.

[36] The FE transition in these classes of materials, however, is expected to be at a much higher temperature than the magnetic transition so it should be kept in mind that this approach teaches us about coupling in the ground state, which is not accessible from a phenomenological model expanded about the FE-AFM phase.